Magnetic Resonance Imaging 57 (2019) 210–217

Contents lists available at ScienceDirect

Magnetic Resonance Imaging

journal homepage: www.elsevier.com/locate/mri

Original contribution

Evaluation of hepatic function using dynamic contrast-enhanced magnetic resonance imaging in melanocortin 4 receptor-deficient mice as a model of nonalcoholic steatohepatitis

Tomomi Yamada[a,*], Yuto Kashiwagi[a], Takemi Rokugawa[a], Hideaki Kato[b], Haruyo Konishi[b], Tadateru Hamada[b], Ryohei Nagai[b], Yusaku Masago[b], Michiko Itoh[c], Takayoshi Suganami[d], Yoshihiro Ogawa[e,f,g], Kohji Abe[a]

[a] Biomarker R&D Department, Shionogi & Co., Ltd., Osaka, Japan
[b] Drug Discovery& Disease Research Laboratory, Shionogi & Co., Ltd., Osaka, Japan
[c] Department of Organ Network and Metabolism, Graduate School of Medicine, Tokyo Medical and Dental University, Tokyo, Japan
[d] Department of Molecular Medicine and Metabolism, Research Institute of Environmental Medicine, Nagoya University, Nagoya, Japan
[e] Department of Medical and Bioregulatory Science, Graduate School of Medical Sciences, Kyushu University, Fukuoka, Japan
[f] Department of Molecular and Cellular Metabolism, Graduate School of Medicine, Tokyo Medical and Dental University, Tokyo, Japan
[g] Japan Agency for Medical Research and Development, CREST, Tokyo, Japan

ARTICLE INFO

Keywords:
Dynamic contrast-enhanced-MRI
Melanocortin 4 receptor-deficient mice
NASH
Gd-EOB-DTPA
High-fat diet

ABSTRACT

Introduction: Melanocortin 4 receptor-deficient (MC4R-KO) mice fed a high-fat diet (HFD) develop liver pathology similar to human nonalcoholic steatohepatitis (NASH). However, although liver histology and blood biochemistry have been reported, hepatic function has not been evaluated. In the present study, we evaluated hepatic function in MC4R-KO mice fed an HFD using dynamic contrast-enhanced magnetic resonance imaging (DCE-MRI) with gadolinium-ethoxybenzyl-diethylenetriamine pentaacetic acid (Gd-EOB-DTPA).

Materials and methods: Wild type (WT) mice and MC4R-KO mice were fed a standard diet (SD) or an HFD for 20 weeks. The hepatic signal intensity was obtained from DCE-MRI images, and relative enhancement (RE), the time to maximum RE (T_{max}), and the half-life of RE elimination ($T_{1/2}$) were calculated. Histopathological analysis was then performed.

Results: Histological analysis with nonalcoholic fatty liver disease activity score (NAS) revealed that MC4R-KO mice fed an HFD achieved the NAS of 5. There was moderate fibrosis in MC4R-KO mice fed an HFD. DCE-MRI with Gd-EOB-DTPA showed that T_{max} and $T_{1/2}$ were significantly longer in MC4R-KO mice fed an HFD compared with wild type (WT) mice (T_{max}, WT, 3.9 ± 0.4 min; MC4R-KO, 7.4 ± 1.5 min; $T_{1/2}$, WT, 23.7 ± 1.9 min; MC4R-KO, 62.5 ± 18.5 min). T_{max} and $T_{1/2}$ were significantly correlated with histopathologic score (steatosis *vs.* Tmax, rho = 0.48, $P = 0.04$; steatosis *vs.* $T_{1/2}$, rho = 0.50, $P = 0.03$; inflammation *vs.* Tmax, rho = 0.55, $P = 0.02$; inflammation *vs.* $T_{1/2}$, rho = 0.61, $P < 0.01$; ballooning *vs.* $T_{1/2}$, rho = 0.51, $P = 0.03$;fibrosis *vs* T_{max}, rho = 0.72, $P < 0.01$; fibrosis *vs* $T_{1/2}$, rho = 0.75, $P < 0.01$).

Conclusions: MC4R-KO mice fed an HFD developed obesity and NASH. The liver kinetics of Gd-EOB-DTPA were significantly different in MC4R-KO mice fed an HFD from WT mice, and correlated with the histopathologic score. These results suggest that MC4R-KO mice fed an HFD mimic the hepatic pathology and liver function of human NASH, and therefore might be useful for the study of hepatic dysfunction during the fibrotic stage of NASH.

Abbreviations: DCE-MRI, dynamic contrast-enhanced magnetic resonance imaging; EMM, empirical mathematical model; Gd-EOB-DTPA, gadolinium-ethoxybenzyl-diethylenetriamine pentaacetic acid; HFD, high-fat diet; IHL, intrahepatic lipid; MC4R-KO mice, melanocortin 4 receptor-deficient mice; NASH, nonalcoholic steatohepatitis; SD, standard diet

* Corresponding author at: Biomarker R&D Department, Shionogi & Co., Ltd., 3-1-1 Futaba, Toyonaka, Osaka 561-0825, Japan.
E-mail address: tomomi.yamada@shionogi.co.jp (T. Yamada).

https://doi.org/10.1016/j.mri.2018.11.013
Received 25 June 2018; Received in revised form 9 October 2018; Accepted 17 November 2018

1. Introduction

Nonalcoholic fatty liver disease (NAFLD) is the most common hepatic disorder in Western countries and its prevalence is rising worldwide, alongside the development of epidemics of obesity and type 2 diabetes mellitus [1–3]. NAFLD encompasses a range of hepatic pathologies, from relatively benign simple steatosis to the more serious nonalcoholic steatohepatitis (NASH), which can progress to liver cirrhosis and hepatocellular carcinoma [1–3]. There is no established evidence-based drug therapy for NASH; therefore, the treatment of NASH represents a significant unmet medical need.

Many animal models have been developed to study the pathogenesis of NASH [4–6], and these are also indispensable for the screening of novel therapies. The pathogenesis of NAFLD/NASH is complex, requiring multiple 'hits', but the underlying risk factors are considered to be those comprising the metabolic syndrome. Various diet-induced obesity (DIO) models have been used that mimic the etiology and natural history of NASH. However, although these models develop steatosis within a few weeks, it takes a considerable period of time for them to develop inflammation and hepatic fibrosis, and the fibrosis that does develop remains mild [7,8]. To reproduce the progressive hepatic fibrosis that reflects human NASH pathology within a shorter timeframe, nutrient-deficiency and chemically induced models are frequently used [4,5]. In particular, the dietary methionine-choline deficiency (MCD) model is the most well-established model for studying the oxidative stress, inflammation, and fibrosis of NAFLD/NASH [9,10]. However, because these mice do not develop obesity, it is not possible to accurately reproduce the pathogenetic mechanism and metabolic status of the human disease in this way.

In addition to environmentally-based NASH models, genetic models (monogenetic or polygenetic) are also widely used in NAFLD/NASH research [4–6]. Although genetic studies of NASH have identified rare monogenic conditions that feature severe NAFLD, heterozygous mutation of the melanocortin-4 receptor (MC4R) is one of the most common monogenic causes of human obesity [11,12], and MC4R-deficient (MC4R-KO) mice are reported to develop obesity, associated with hyperphagia, hyperinsulinemia, and hyperglycemia [13]. Furthermore, these MC4R-KO mice exhibit NASH pathology when fed a high-fat diet (HFD) [14,15]. When MC4R-KO mice are fed an HFD, they exhibit biochemical and hepatopathological features of NASH and altered expression of lipid metabolism genes [14,16,17]. Furthermore, the livers of the mice develop fibrosis and well-differentiated hepatocellular carcinomas after a longer period of time [14]. MC4R-KO mice reproduce human NASH disease in many respects of pathophysiological mechanisms and metabolic status. Thus, the MC4R-KO mouse is a valuable research model that provides insight into the pathogenetic mechanism and treatment of NASH.

Gadolinium-ethoxybenzyl-diethylenetriamine pentaacetic acid (Gd-EOB-DTPA), a hepatobiliary contrast agent for magnetic resonance imaging (MRI), is widely used for the diagnosis of liver tumors and other focal lesions [18–20]. Gd-EOB-DTPA enhancement of the hepatic parenchyma depends on the functional integrity of hepatocytes, and therefore Gd-EOB-DTPA-enhanced MRI can be used for the evaluation of liver function. In human studies, the degree of relative enhancement (RE) or rate of reduction of T1 values in the liver after Gd-EOB-DTPA injection has been shown to be potentially useful for the estimation of hepatic function, and the diagnosis of NASH and liver fibrosis [21–25]. Studies in animal models have demonstrated that it is possible to assess hepatic function and the progression of liver fibrosis in NASH by evaluating the signal profile of the RE of Gd-EOB-DTPA [26–28]. We have also reported that changes in Gd-EOB-DTPA kinetics are significantly correlated with hepatic inflammation in MCD diet-fed mice [28]. Thus, Gd-EOB-DTPA-enhanced MRI is used to evaluate liver pathophysiology of NASH in pre-clinical and clinical studies, suggesting that it is a non-invasive translational research tool. To our knowledge, although the histologic and biochemical characteristics of MC4R-KO mice have been studied, the liver function of these mice has not been fully evaluated when NASH has developed.

The purpose of our study was to evaluate hepatic function using Gd-EOB-DTPA-enhanced MRI in MC4R-KO mice fed an HFD and to compare the results generated with the staging of NAFLD by histopathologic examination.

2. Materials and methods

All experimental protocols were approved by the Institutional Animal Care and Use Committee of Shionogi Research Laboratories.

2.1. Generation of Mc4r knockout mice

We designed a targeting vector that would replace all of the protein coding region of exon 1 of the murine *Mc4r* gene with a neomycin resistance cassette, in order to completely inactivate it. The targeting vector was electroporated into C57BL/6J mouse embryonic stem (ES) cells that were established by previous method [29]. After neomycin resistance selection with G418, stem cell clones that had undergone homologous recombination were screened by PCR and Southern blotting analysis. Chimeric mice were generated from heterozygous ES clones by aggregation, and the chimeras obtained were bred with C57BL/6J (CLEA Japan Inc., Shizuoka, Japan) mice to establish *Mc4r*-deficient heterozygous mice. *Mc4r*-deficient homozygous (MC4R-KO) mice and wild-type (WT) mice were obtained by heterozygous intercrosses.

2.2. Animal model

During the entire study period, the mice were maintained under standard conditions. They were allowed free access to chow and tap water and were housed in a temperature-controlled room maintained on a 12-h light/dark cycle, with lights on at 08:00. In the HFD-feeding experiments, 8-week-old male mice were give free access to water and either standard diet (SD) (CE-2, 12.1% kcal from fat) (Clea Japan Inc., Tokyo, Japan) or HFD (D12492, 60.0% kcal from fat) (Research Diets Inc., New Brunswick, NJ, USA) for 20 weeks.

2.3. ^{1}H-magnetic resonance spectroscopy and magnetic resonance imaging

All magnetic resonance spectroscopy (MRS) and MRI examinations were performed in mice anesthetized with 1–2% isoflurane delivered through a face mask, with respiratory monitoring. Core body temperature was monitored with a rectal fiber-optic probe (SA Instruments, NY, USA) and maintained at 37.0 ± 0.5 °C by blowing warm air into the magnet. All MRS and MRI measurements were performed with a Varian MRI System 7T/210 (Agilent, CA, USA) controlled by VNMRJ software. A 63-mm volume coil was used for radiofrequency (RF) transmission and reception.

The spin echo sequence was used for liver anatomical reference imaging with respiratory triggering. The parameters were as follows: field of view, 40 × 40 mm^2; matrix, 128 × 128; repetition time/echo time, 500/24.5 msec; number of acquisitions, 2; number of slices, 8; and slice thickness, 2 mm without a gap. Localized ^{1}H-MRS traces were obtained from 8 mm^3 volumes in two deep sites in the liver, adjacent to the portal vein. Single-voxel localized ^{1}H-MRS traces were acquired using a steam sequence, with respiratory triggering. The parameters were as follows: repetition time/echo time/mixing time, 1200/10/8 msec; number of acquisitions, 64; real points, 2000; spectral width, 4006 Hz. A non-water-suppressed spectrum was recorded within the same voxel with 4 acquisitions, yielding a water reference signal.

DCE-MRI measurements were performed using a T1-weighted gradient echo sequence without respiratory triggering. The parameters were as follows: repetition time/echo time, 39.06/1.42 msec; flip angle, 36°; field of view, 40 × 40 mm^2; matrix, 128 × 128; number of slices,

8; slice thickness, 2 mm without gap. Then, 120 s after the start of the scan, Gd-EOB-DTPA (0.025 mmol Gd/kg body mass was injected into the tail vein *via* a 27-gauge indwelling catheter connected to an extension tube. In total, 141 scans, including 6 pre-contrast measurements, were obtained at intervals of 20 s for up to 47 min.

2.4. Histopathological analysis

After MRI study, mice were sacrificed by exsanguination under isoflurane anesthesia. The left lateral liver lobes were fixed in phosphate-buffered 10% formalin, and the sections were stained with hematoxylin and eosin (HE) or Sirius-red. The HE-stained specimens were scored according to the NAFLD activity score (NAS), comprising the sum of the scores for steatosis (0–3), lobular inflammation (0–3), and hepatocellular ballooning (0–2). The Sirius red-positive area was measured using image analysis software (WinROOF; Mitani Corporation, Tokyo, Japan). Histological assessment and scoring were performed blind.

2.5. Data analysis

Liver fat content was estimated using spectral analysis by LCModel (version 6.3-1J, Stephen Provencher, Oakville, ON, Canada). 'Liver 7' was used as the base, with all signals occurring in the spectral range of −2–8 ppm simulated in LCModel. From the LCModel analysis, the areas of the lipid peaks (*L*) at 1.3, 0.9, and 1.6 ppm, including those representing both the methyl and methylene groups of the triglyceride molecule, and the area of the water peak (*W*), were used to quantify the lipid content of the liver [30]. Intrahepatic lipid (*IHL*) was calculated using the following equation:

$$IHL = [L/(L + W)] \times 100\,(\%)$$

A region of interest (ROI) with an area of 312–317 pixels (mean 314 pixels) was drawn on one slice image that included liver parenchyma and no vascular component using ImageJ software (Rasband, W.S., ImageJ, U. S. National Institutes of Health, Bethesda, Maryland, USA, http://imagej.nih.gov/ij/). Signal intensity (SI) values for the liver were measured for each MR image, and RE was calculated using the following equation:

$$RE(t) = [(SI(t) - SI(0))/(SI(0))] \times 100\,(\%), \quad (1)$$

where *SI(t)* is the SI of the liver after injection of Gd-EOB-DTPA and *SI (0)* is the average pre-contrast SI. The time course of liver *RE* was fitted using an empirical mathematical model (EMM) [31]:

$$RE(t) = \begin{cases} 0 & 0 \le t < t_0 \\ A \cdot [1 - e^{-\alpha(t-t_0)}]^q \cdot e^{-\beta(t-t_0)} & t_0 \le t \end{cases} \quad (2)$$

where A is the upper limit of the RE, α is the rate of contrast uptake (min^{-1}), β is the rate of contrast washout (min^{-1}), q is a parameter related to the slope of the early uptake, and t_0 is the rise time point (min). The time to maximum *RE* (T_{max}) and the half-life of the elimination *RE* ($T_{1/2}$) were calculated from the fitted curve. In addition, T_{max} and $T_{1/2}$ maps were obtained by calculation on a pixel-by-pixel basis.

2.6. Statistical analysis

All data are expressed as mean ± SE. Differences in body mass, liver mass, IHL, Sirius red-positive area, T_{max}, and $T_{1/2}$ of the time course of RE in the liver in each group were analyzed by two-way analysis of variance and the Tukey-Kramer test. The differences in histological scores were assessed using the Steel-Dwass multiple comparison test. Spearman's rank correlation was used to evaluate the relationship between the DCE-MRI results and liver histology scores. A value of $P < 0.05$ was considered to represent a statistically significant difference.

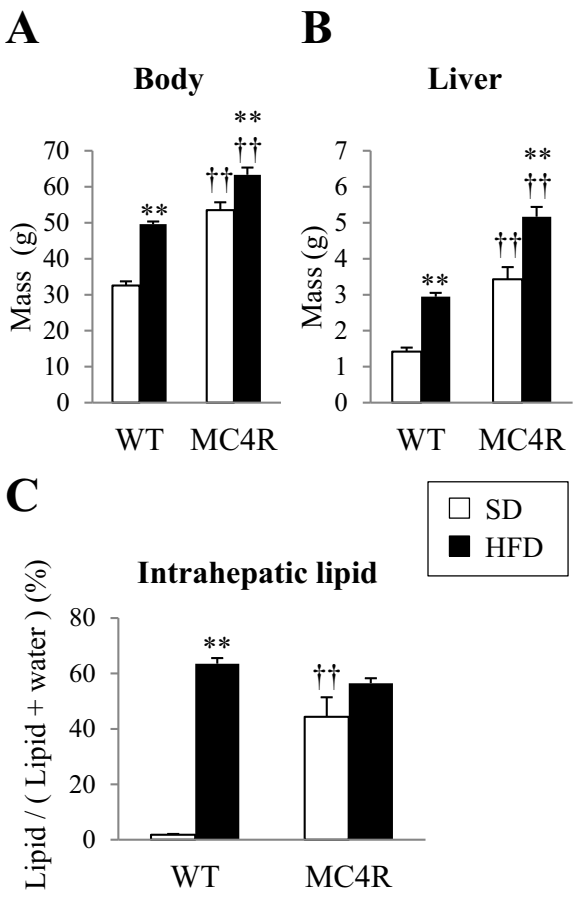

Fig. 1. Body and liver masses of WT and MC4R-KO mice.
Masses of the body (A) and liver (B) in wild-type (WT) and MC4R-KO (MC4R) mice fed either a standard diet (SD) or a high-fat diet (HFD) (mean ± SE). C: Intrahepatic lipid after 20 weeks of diet feeding (mean ± SE). ††$P < 0.01$ *versus* diet-matched control; **$P < 0.01$ *versus* genotype-matched control. Wild-type mice fed the standard diet (n = 5); wild-type mice fed the high-fat diet (n = 5); MC4R-KO mice fed the standard diet (n = 5); MC4R-KO mice fed the high-fat diet (n = 4).

3. Results

3.1. Histopathological phenotype and MRS of the MC4R-KO mice

After 20 weeks' consumption of an SD or an HFD, both body and liver masses of the MC4R-KO mice were significantly greater ($P < 0.01$) than those of the WT mice (Fig. 1A and B). WT mice fed the HFD and MC4R-KO mice fed the SD had significantly higher IHL ratios than WT mice fed the SD ($P < 0.01$). MC4R-KO mice fed the HFD showed a similar IHL ratio to WT mice fed the HFD (Fig. 1C).

The histopathologic data show that severe hepatic steatosis and moderate inflammation were present in livers from WT mice fed the HFD and MC4R-KO mice fed both diets (Fig. 2A). Livers from all MC4R-KO mice fed the HFD exhibited hepatocyte ballooning degeneration (Fig. 2A). Histological scoring of NAFLD revealed that MC4R-KO mice fed the HFD were the only group to achieve a NAS of 5 (Table 1). Sirius red staining showed significant periportal and/or perisinusoidal fibrosis in livers from MC4R-KO mice fed the HFD (Fig. 2B), whereas there was only slight fibrosis in WT mice fed the HFD and MC4R-KO mice fed the SD.

3.2. Time course of RE in DCE-MRI

Initially, we found that there were significant differences between

WT mice fed the SD and the other groups in baseline pre-contrast SI in the liver (pre-contrast SI: WT-SD, 1803 ± 41; WT-HFD, 564 ± 11, $P < 0.0001$; MC4R-SD, 885 ± 128, $P < 0.0001$; MC4-HFD, 624 ± 37, $P < 0.0001$) (Fig. 3A). Therefore, we assessed the kinetics

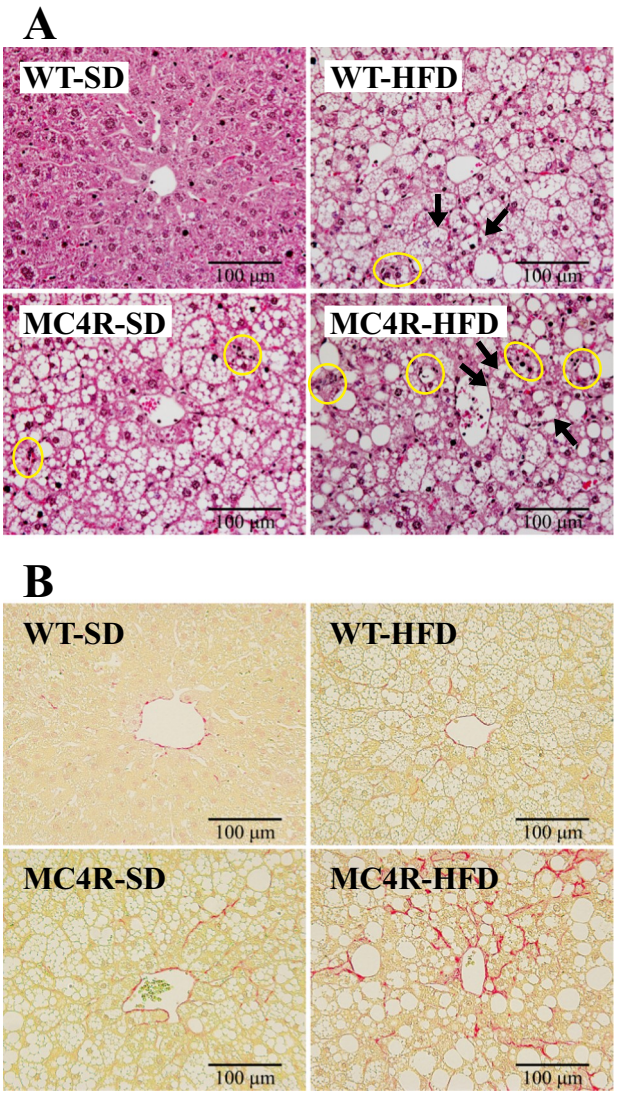

Fig. 2. Liver histology of WT and MC4R-KO mice.
Hematoxylin and eosin (HE) staining (A) and Sirius red staining (B) of liver sections from wild-type (WT) and MC4R-KO (MC4R) mice fed either the standard diet (SD) or the high-fat diet (HFD). Liver sections were stained with HE in order to evaluate the NAFLD activity score. Original magnification, ×200. Yellow circle, infiltrated inflammatory cells; arrowhead, hepatocyte ballooning. (C): Quantification of the area positive for Sirius red (mean ± SE). †$P < 0.05$ *versus* diet-matched control; *$P < 0.05$ *versus* genotype-matched control. WT-SD, wild-type mice fed the standard diet (n = 5); WT-HFD, wild-type mice fed the high-fat diet (n = 5); MC4R-SD, MC4R-KO mice fed the standard diet (n = 5); MC4R-HFD, MC4R-KO mice fed the high-fat diet (n = 4).

Table 1
NAFLD activity score (NAS) in WT and MC4R-KO mice.

	WT		MC4R-KO	
	SD (n = 5)	HFD (n = 5)	SD (n = 5)	HFD (n = 4)
Steatosis	0.0 ± 0.0	2.2 ± 0.2*	1.6 ± 0.2†	2.0 ± 0.0
Inflammation	0.2 ± 0.2	1.4 ± 0.2	1.4 ± 0.2	2.0 ± 0.0
Ballooning	0.0 ± 0.0	0.6 ± 0.4	0.0 ± 0.0	1.5 ± 0.3*
NAS	0.2 ± 0.2	4.2 ± 0.6*	3.0 ± 0.3†	5.5 ± 0.3
NASH	0/5	2/5	0/5	4/4

Total NAS score is the sum of the values recorded for each category. NAS total score interpretation: 1–2 = no NASH; 3–4 = borderline; 5–8 = NASH. †$P < 0.05$ *versus* diet-matched control; *$P < 0.05$ *versus* genotype-matched control. WT, wild-type mice; MC4R-KO, MC4R-KO mice; SD, standard diet; HFD, high-fat diet.

(T_{max} and $T_{1/2}$) of RE in this study, because the relationship between the concentration of contrast agent and RE might be affected by differences in baseline SI. Fig. 3B shows the time course of RE in the liver after administration of Gd-EOB-DTPA to WT and MC4R-KO mice. In WT mice fed the SD, RE increased immediately after Gd-EOB-DTPA administration and was lost over the following 40 min. In MC4R-KO mice fed the HFD, RE showed delayed peaks, and slower decay of RE was observed.

Fig. 4 show the T_{max} and $T_{1/2}$ values that were calculated from the time course of RE for each individual region of interest (ROI) (Fig. 3A) in each group. T_{max} and $T_{1/2}$ were significantly prolonged in MC4R-KO mice fed the HFD compared with WT mice fed the HFD (T_{max}, WT-HFD, 3.9 ± 0.4 min; MC4R-KO-HFD, 7.4 ± 1.5 min, $P < 0.05$, Fig. 4A; $T_{1/2}$, WT-HFD, 23.7 ± 1.9 min; MC4R-KO-HFD, 62.5 ± 18.5 min, $P < 0.05$, Fig. 4B). Fig. 5 shows typical T_{max} and $T_{1/2}$ maps, generated on a pixel-by-pixel basis, for each group. T_{max} and $T_{1/2}$ were prolonged in the entire liver parenchyma for WT mice fed the HFD and MC4R-KO mice fed both diets.

3.3. Correlation between Gd-EOB-DTPA kinetics and NAFLD activity score in the liver

We next evaluated the relationship between the DCE-MRI results and the scores for hepatic steatosis, lobular inflammation, and ballooning degeneration, and the fibrosis (Sirius red-positive area ratio) in the liver. T_{max} showed positive correlations with the degree of histological steatosis, inflammation, and fibrosis (steatosis, rho = 0.48, $P = 0.04$; inflammation, rho = 0.55, $P = 0.02$; fibrosis, rho = 0.72, $P = 0.001$, Fig. 6A). $T_{1/2}$ also showed positive correlations with all the histological scores (steatosis, rho = 0.50, $P = 0.03$; inflammation, rho = 0.61, $P = 0.005$; ballooning, rho = 0.51, $P = 0.03$; fibrosis, rho = 0.75, $P = 0.0002$, Fig. 6B).

4. Discussion

In this study, MC4R-KO mice had significantly higher body mass than WT mice and showed obvious obesity (Fig. 1). The MC4R is a seven-transmembrane G protein-coupled receptor that is expressed in

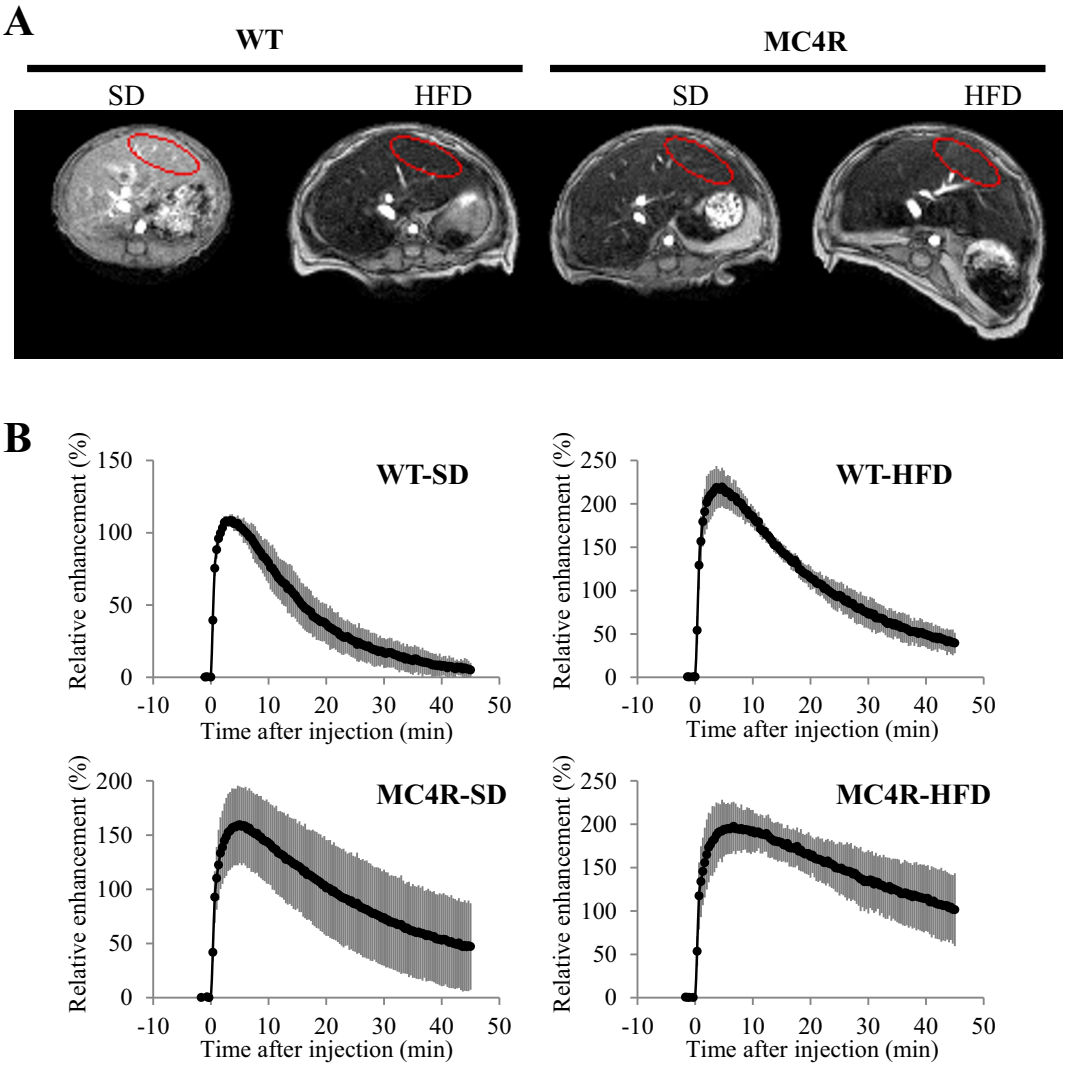

Fig. 3. The time course of relative enhancement in the liver before and after Gd-EOB-DTPA injection in WT and MC4R-KO mice.
Typical regions of interest placed on pre-contrast images for each group (A). The red lines represent the regions of interest. The time course of relative enhancement (RE) in the liver (mean ± SE) for each group before and after injection of Gd-EOB-DTPA at 0.025 mmol Gd/kg (B). WT-SD, wild-type mice fed the standard diet (n = 5); WT-HFD, wild-type mice fed the high-fat diet (n = 5); MC4R-SD, MC4R-KO mice fed the standard diet (n = 5); MC4R-HFD, MC4R-KO mice fed the high-fat diet (n = 4).

hypothalamic nuclei and is implicated in the regulation of food intake and body weight [32]. MC4R mutations are the most commonly recognized monogenic cause of obesity in humans and mice [6,11–13]. The NAS in all of the MC4R-KO mice fed an HFD for 20 weeks were > 5 (Fig. 2, Table 1), whereas it was 3–6 in WT mice fed an HFD (Fig. 2, Table 1). Because WT mice fed an HFD exhibited similar increases in steatosis and inflammation scores to MC4R-KO mice fed an HFD there was no significant difference in NAS between these groups. However, only MC4R-KO mice fed an HFD exhibited marked hepatic fibrosis (Fig. 2), implying that MC4R-KO mice fed an HFD for 20 weeks develop progressive NASH, whereas WT mice fed an HFD for 20 weeks develop severe steatosis or non-progressive NASH. These results are consistent with a previous report showing that MC4R-KO mice fed an HFD exhibit obvious fibrosis, whereas WT mice fed an HFD do not [14]. Furthermore, MC4R-KO mice fed an HFD have been reported to demonstrate very similar hepatopathological features of NASH with fibrosis to humans [14,15]. Thus, the MC4R-KO mouse fed an HFD is a model of NASH that reproduces both the obesity and the progressive hepatic fibrosis seen in humans. Therefore, this model should be very useful for the study of mechanisms involved in the progression of simple steatosis to NASH.

Recently, Gd-EOB-DTPA-enhanced MRI has been identified as a promising method for the characterization of liver function and staging of liver fibrosis in animal models and humans [21–28]. Several studies have used relative enhancement by Gd-EOB-DTPA as an index of liver function [23,24]. However, if the relaxation time of the liver itself changes, the signal enhancement by Gd-EOB-DTPA may change, even when assessed using the same MRI system. Therefore, in recent years, Gd-EOB-DTPA-enhanced T1 mapping technology has been studied as a quantitative method for the evaluation of liver disease [25]. However, small animals cannot be made to breath-hold during an MRI scan, making accurate T1 mapping challenging. Conversely, although RE can be semi-quantitative, depending on the experimental conditions, because the temporal transition of the signal intensity after the administration of a contrast agent is not affected by the relaxation time at baseline, kinetic analysis is useful for the evaluation of liver function [21,22,27,28]. In this study, the T_{max} and $T_{1/2}$ of the DCE-MRI in MC4R-KO mice fed an HFD were significantly prolonged *versus* those of the WT mice fed an HFD, after Gd-EOB-DTPA injection (Fig. 4). Comparisons between DCE-MRI parameters and hepatic histopathological evaluation showed that T_{max} and $T_{1/2}$ correlated with steatosis score, inflammation score, and the severity of fibrosis (Fig. 6). Tsuda et al.

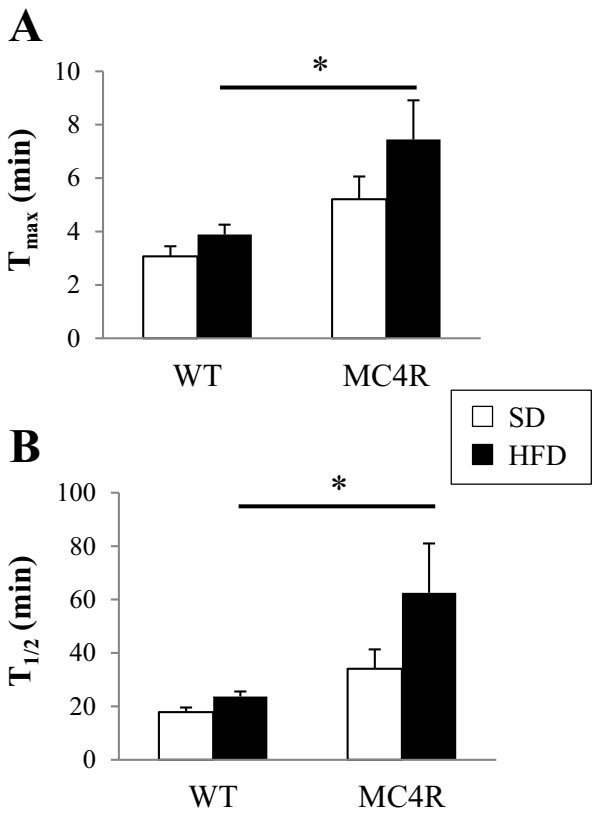

Fig. 4. T_{max} and $T_{1/2}$ after Gd-EOB-DTPA injection in WT and MC4R-KO mice. Comparison of T_{max} (B) and $T_{1/2}$ (C) in each group (mean ± SE). WT, wild-type mice; MC4R, MC4R-KO mice; SD, standard diet; HFD, high-fat diet. Wild-type mice fed the standard diet (n = 5); wild-type mice fed the high-fat diet (n = 5); MC4R-KO mice fed the standard diet (n = 5); MC4R-KO mice fed the high-fat diet (n = 4).

previously reported that prolongation of T_{max} and $T_{1/2}$ on Gd-EOB-DTPA-enhanced MRI correlates with fibrosis in nutrient-deficient dietary NASH models [27], and suggested this prolongation was caused by the suppression of biliary excretion in NASH with fibrosis.

In several clinical studies, it has been reported that the RE of Gd-EOB-DTPA in hepatic parenchyma decreases as NASH and liver fibrosis progresses [21–25]. In addition, and especially in patients with NASH, the RE of Gd-EOB-DTPA in the liver has been reported to be negatively correlated with the degree of inflammation, ballooning, and fibrosis, but not with steatosis [23]. Finally, in patients with moderate fibrosis (stage F1 or F2), inflammation and cholestasis in the liver have been suggested to cause accumulation of Gd-EOB-DTPA in hepatocytes [24]. These clinical findings imply that uptake of Gd-EOB-DTPA into hepatocytes is inhibited in steatohepatitis with fibrosis and also that the elimination of Gd-EOB-DTPA in the bile is suppressed in the presence of moderate fibrosis. Thus, in NASH with moderate fibrosis, T_{max} and $T_{1/2}$ are considered to lengthen. In this study, MC4R-KO mice fed an HFD exhibited periportal and/or perisinusoidal fibrosis corresponding to fibrosis stage 1 or 2 in the scoring system for human NASH. Thus, the MC4R-KO mice fed an HFD for 20 weeks are a NASH model which functionally mimics the human disease state of NASH, with moderate fibrosis developing in this study.

Gd-EOB-DTPA is taken up selectively by hepatocytes and subsequently excreted into the bile by transporters. It is well known that the organic anion transporting polypeptide 1 mediates the uptake, and that multidrug resistance protein 2 mediates the biliary excretion of Gd-EOB-DTPA [18–20]. The degree of enhancement and signal prolongation of Gd-EOB-DTPA are affected by the expression level of these hepatic transporters. Inflammatory cytokines have been reported to suppress hepatic transporter expression [33] and we have recently reported that the kinetics of Gd-EOB-DTPA in the liver, assessed using DCE-MRI, correlate with the hepatic inflammation score in mice fed an MCD diet [28]. The expression of hepatic transporters may be altered by inflammatory cytokines secreted as part of the inflammatory process in the liver. In this study, the T_{max} and $T_{1/2}$ for Gd-EOB-DTPA in the DCE-MRI of MC4R-KO mice fed an HFD were significantly prolonged in comparison with those of WT mice fed an HFD (Fig. 4). In addition, although fibrosis was significantly greater in MC4R-KO mice fed an HFD than in similarly fed WT mice, there was no significant difference in inflammation score between these groups (Table 1). The deposition of extracellular collagen during fibrosis may impede the diffusion and uptake of Gd-EOB-DTPA [22,24]. Therefore, it is likely that the kinetics of Gd-EOB-DTPA would only have been significantly altered in MC4R-KO mice fed an HFD that had marked liver fibrosis. Moreover, in MC4R-KO mice fed an HFD, it is likely that other factor s would also have

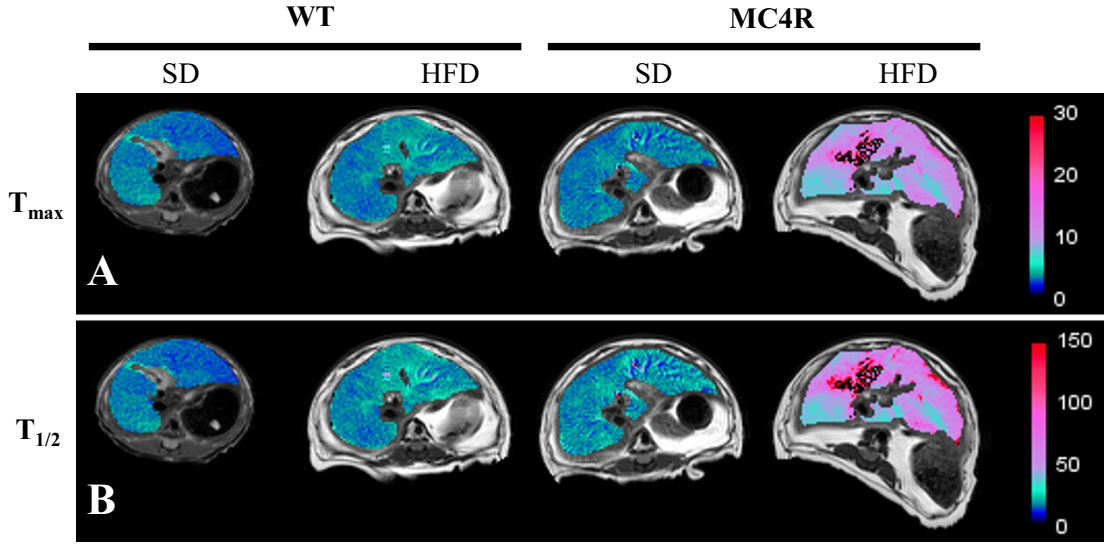

Fig. 5. Typical T_{max} and $T_{1/2}$ maps for WT and MC4R-KO mice.
Typical T_{max} (A) and $T_{1/2}$ (B) maps, generated on a pixel-by-pixel basis, for each group. WT, wild-type mice; MC4R, MC4R-KO mice; SD, standard diet; HFD, high-fat diet.

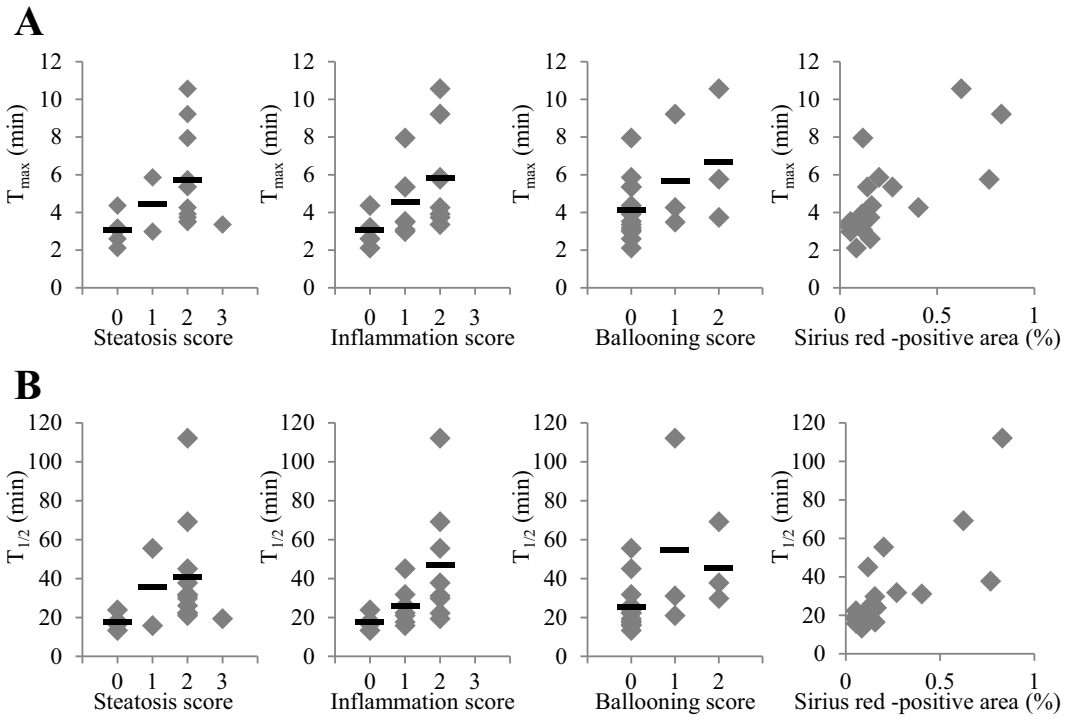

Fig. 6. Correlations between kinetic parameters for DCE-MRI with Gd-EOB-DTPA and histopathological score in each group.
Correlation between T_{max} and steatosis score (rho = 0.48, P = 0.04), correlation between T_{max} and inflammation score (rho = 0.55, P = 0.02), correlation between T_{max} and ballooning score (rho = 0.42, P = 0.08), correlation between T_{max} and Sirius red positive area (rho = 0.72, P = 0.001) (A). Correlation between $T_{1/2}$ and steatosis score (rho = 0.50, P = 0.03), correlation between $T_{1/2}$ and inflammation score (rho = 0.61, P = 0.005), correlation between $T_{1/2}$ and ballooning score (rho = 0.51, P = 0.03), correlation between $T_{1/2}$ and Sirius red positive area (rho = 0.75, P = 0.0002) (B). Horizontal bars represent mean values.

affected the kinetics of Gd-EOB-DTPA. Itoh et al. reported that tumor necrosis factor α (TNF-α) mRNA expression was high in the livers of both MC4R-KO and WT mice fed an HFD, whereas TNF-α mRNA expression in white adipose tissue and serum interleukin-6 were much higher in MC4R-KO mice than in WT mice fed an HFD [14]. Higher circulating levels of inflammatory cytokines may contribute to the suppression of hepatic transporter expression [34]. Itoh et al. considered that enhanced adipose tissue inflammation has a role in both the first and second hits involved in the development of NASH in MC4R-KO mice [14]. In MC4R-KO mice fed an HFD, the enhanced adipose tissue inflammation may promote NASH progression, induce fibrosis, and at the same time reduce the expression of hepatic transporters. Further experiments are required to clarify the role of inflammatory cytokines and transporters in the kinetics of Gd-EOB-DTPA in the liver of MC4R-KO mice.

5. Conclusion

The liver kinetics of Gd-EOB-DTPA are significantly different in MC4R-KO mice fed an HFD to those in WT mice consuming the same diet, and correlate with the degrees of inflammation and fibrosis. This study shows that MC4R-KO mice fed an HFD developed obesity and NASH with fibrosis, which functionally mimics the human NASH disease state. These results suggest that MC4R-KO mice fed an HFD should be useful for the study of hepatic dysfunction in the fibrotic stage of NASH. In addition, MRI-based techniques that can be used for both mouse and human are available to bridge the gap between animal model experiments and clinical trials as a substitute for liver histology in the development of new drugs.

Acknowledgment

We thank Mark Cleasby, PhD, from Edanz Group (www.edanzediting.com/ac) for editing a draft of this manuscript.

Declaration of interest

Michiko Itoh is assigned to Joint Research Department of Tokyo Medical and Dental University and Shionogi & Co. Ltd.

References

[1] Bellentani S. The epidemiology of non-alcoholic fatty liver disease. Liver Int 2017;37:81–4.
[2] Tilg H, Moschen AR, Roden M. NAFLD and diabetes mellitus. Nat Rev Gastroenterol Hepatol 2017;14(1):32–42.
[3] Vernon G, Baranova A, Younossi ZM. Systematic review: the epidemiology and natural history of non-alcoholic fatty liver disease and non-alcoholic steatohepatitis in adults. Aliment Pharmacol Ther 2011;34(3):274–85.
[4] Anstee QM, Goldin RD. Mouse models in non-alcoholic fatty liver disease and steatohepatitis research. Int J Exp Pathol 2006;87(1):1–16.
[5] Hansen HH, Feigh M, Veidal SS, Rigbolt KT, Vrang N, Fosgerau K. Mouse models of nonalcoholic steatohepatitis in preclinical drug development. Drug Discov Today 2017;22(11):1707–18.
[6] Mann JP, Semple RK, Armstrong MJ. How useful are monogenic rodent models for the study of human non-alcoholic fatty liver disease? Front Endocrinol 2016;7(NOV).
[7] DeLeve LD, Wang X, Kanel GC, Atkinson RD, McCuskey RS. Prevention of hepatic fibrosis in a murine model of metabolic syndrome with nonalcoholic steatohepatitis. Am J Pathol 2008;173(4):993–1001.
[8] Ito M, Suzuki J, Tsujioka S, Sasaki M, Gomori A, Shirakura T, et al. Longitudinal analysis of murine steatohepatitis model induced by chronic exposure to high-fat diet. Hepatol Res 2007;37(1):50–7.
[9] Kirsch R, Clarkson V, Shephard EG, Marais DA, Jaffer MA, Woodburne VE, et al.

Rodent nutritional model of non-alcoholic steatohepatitis: species, strain and sex difference studies. J Gastroenterol Hepatol 2003;18(11):1272–82.
[10] Leclercq IA, Farrell GC, Field J, Bell DR, Gonzalez FJ, Robertson GR. CYP2E1 and CYP4A as microsomal catalysts of lipid peroxides in murine nonalcoholic steatohepatitis. J Clin Invest 2000;105(8):1067–75.
[11] Farooqi IS, Keogh JM, Yeo GSH, Lank EJ, Cheetham T, O'Rahilly S. Clinical spectrum of obesity and mutations in the melanocortin 4 receptor gene. N Engl J Med 2003;348(12):1085–95.
[12] Vaisse C, Clement K, Durand E, Hercberg S, Guy-Grand B, Froguel P. Melanocortin-4 receptor mutations are a frequent and heterogeneous cause of morbid obesity. J Clin Invest 2000;106(2):253–62.
[13] Huszar D, Lynch CA, Fairchild-Huntress V, Dunmore JH, Fang Q, Berkemeier LR, et al. Targeted disruption of the melanocortin-4 receptor results in obesity in mice. Cell 1997;88(1):131–41.
[14] Itoh M, Suganami T, Nakagawa N, Tanaka M, Yamamoto Y, Kamei Y, et al. Melanocortin 4 receptor-deficient mice as a novel mouse model of nonalcoholic steatohepatitis. Am J Pathol 2011;179(5):2454–63.
[15] Itoh M, Kato H, Suganami T, Konuma K, Marumoto Y, Terai S, et al. Hepatic crown-like structure: a unique histological feature in non-alcoholic steatohepatitis in mice and humans. PLoS One 2013;8(12).
[16] Sutton GM, Trevaskis JL, Hulver MW, McMillan RP, Markward NJ, Babin MJ, et al. Diet-genotype interactions in the development of the obese, insulin-resistant phenotype of C57BL/6J mice lacking melanocortin-3 or -4 receptors. Endocrinology 2006;147(5):2183–96.
[17] Albarado DC, McClaine J, Stephens JM, Mynatt RL, Ye J, Bannon AW, et al. Impaired coordination of nutrient intake and substrate oxidation in melanocortin-4 receptor knockout mice. Endocrinology 2004;145(1):243–52.
[18] Hammerstingl R, Huppertz A, Breuer J, Balzer T, Blakeborough A, Carter R, et al. Diagnostic efficacy of gadoxetic acid (Primovist)-enhanced MRI and spiral CT for a therapeutic strategy: comparison with intraoperative and histopathologic findings in focal liver lesions. Eur Radiol 2008;18(3):457–67.
[19] Reimer P, Schneider G, Schima W. Hepatobiliary contrast agents for contrast-enhanced MRI of the liver: properties, clinical development and applications. Eur Radiol 2004;14(4):559–78.
[20] Reimier P, Rummeny EJ, Daldrup HE, Hesse T, Balzer T, Tombach B, et al. Enhancement characteristics of liver metastases, hepatocellular carcinomas, and hemangiomas with Gd-EOB-DTPA: preliminary results with dynamic MR imaging. Eur Radiol 1997;7(2):275–80.
[21] Saito K, Ledsam J, Sourbron S, Hashimoto T, Araki Y, Akata S, et al. Measuring hepatic functional reserve using low temporal resolution Gd-EOB-DTPA dynamic contrast-enhanced MRI: a preliminary study comparing galactosyl human serum albumin scintigraphy with indocyanine green retention. Eur Radiol 2014;24(1):112–9.
[22] Chen B, Hsu C, Yu C, Wei S, Kao J, Lee H, et al. Dynamic contrast-enhanced magnetic resonance imaging with Gd-EOB-DTPA for the evaluation of liver fibrosis in chronic hepatitis patients. Eur Radiol 2012;22(1):171–80.
[23] Bastati N, Feier D, Wibmer A, Traussnigg S, Balassy C, Tamandl D, et al. Noninvasive differentiation of simple steatosis and steatohepatitis by using gadoxetic acid-enhanced MR imaging in patients with nonalcoholic fatty liver disease: a proof-of-concept study. Radiology 2014;271(3):739–47.
[24] Feier D, Balassy C, Bastati N, Stift J, Badea R, Ba-Ssalamah A. Liver fibrosis: histopathologic and biochemical influences on diagnostic efficacy of hepatobiliary contrast-enhanced MR imaging in staging. Radiology 2013;269(2):460–8.
[25] Haimerl M, Verloh N, Zeman F, Fellner C, Müller-Wille R, Schreyer AG, et al. Assessment of clinical signs of liver cirrhosis using T1 mapping on Gd-EOB-DTPA-enhanced 3T MRI. PLoS One 2013;8(12).
[26] Ryeom H, Kim S, Kim J, Kim H, Lee J, Chang Y, et al. Quantitative evaluation of liver function with MRI using Gd-EOB-DTPA. Korean J Radiol 2004;5(4):231–9.
[27] Tsuda N, Okada M, Murakami T. New proposal for the staging of nonalcoholic steatohepatitis: evaluation of liver fibrosis on Gd-EOB-DTPA-enhanced MRI. Eur J Radiol 2010;73(1):137–42.
[28] Yamada T, Obata A, Kashiwagi Y, Rokugawa T, Matsushima S, Hamada T, et al. Gd-EOB-DTPA-enhanced-MR imaging in the inflammation stage of nonalcoholic steatohepatitis (NASH) in mice. Magn Reson Imaging 2016;34(6):724–9.
[29] Nanchi I, Yoshimura Y, Nakamura K, Masago Y, Ohbayashi T, Okuda T. Exploring new gene integration sites for gene knock-in by gene-trapping strategy. Transgenic Res 2015;24(3):549–59.
[30] Bozzetto L, Prinster A, Annuzzi G, Costagliola L, Mangione A, Vitelli A, et al. Liver fat is reduced by an isoenergetic MUFA diet in a controlled randomized study in type 2 diabetic patients. Diabetes Care 2012;35(7):1429–35.
[31] Moriyama Y, Saito S, Kobayashi S, Ogihara R, Koto D, Kitamura A, et al. Evaluation of concanavalin a-induced acute liver injury in rats using an empirical mathematical model and dynamic contrast-enhanced MR imaging with Gd-EOB-DTPA. Magn Reson Med Sci 2012;11(1):53–60.
[32] Balthasar N, Dalgaard LT, Lee CE, Yu J, Funahashi H, Williams T, et al. Divergence of melanocortin pathways in the control of food intake and energy expenditure. Cell 2005;123(3):493–505.
[33] Fardel O, Le Vée M. Regulation of human hepatic drug transporter expression by pro-inflammatory cytokines. Expert Opin Drug Metab Toxicol 2009;5(12):1469–81.
[34] Hartmann G, Cheung AKY, Piquette-Miller M. Inflammatory cytokines, but not bile acids, regulate expression of murine hepatic anion transporters in endotoxemia. J Pharmacol Exp Ther 2002;303(1):273–81.